NGI Technical note

To:	NVE
Attn.:	Odd-Arne Jensen
Copy to:	
Date:	2022-03-22
Rev. no./Rev.date:	0 /
Document no.:	20200017-09-TN
Project:	AARN - Applied Avalanche Research in Norway
Project manager:	Christian Jaedicke
Prepared by:	Peter Gauer
Reviewed by:	Krister Kristensen

CPT 3 – Quantitative risk assessment

Remarks on the uncertainty in the delimitation of hazard zones based on historical observations

Contents

Review and reference page

NORWEGIAN GEOTECHNICAL INSTITUTE
NGI.NO

Main office
PO Box 3930 Ullevaal St.
NO-0806 Oslo
Norway

Trondheim office
PO Box 5687 Torgarden
NO-7485 Trondheim
Norway

T 22 02 30 00
F 22 23 04 48
NGI@ngi.no

BIC NO. DNBANOKK
IBAN NO26 5096 05 01281
ORGANISATION NO.
958 254 318MVA

ISO 9001/14001
CERTIFIED BY BSI
FS 32989/EMS 612006

1 Introduction

The Norwegian building code regulates the societal acceptable risk from avalanches for three building classes (S1, S1, and S3). The corresponding highest allowed nominal annual probabilities of avalanches reaching the building for these classes are set as 1/100, 1/1000 and 1/5000 respectively (TEK17, 2017). That is, avalanches should not reach a building, or the accompanying outdoor area and cause (considerable) damage more often than the building class permits. These hazard classes are used for delineation of avalanche hazard zones for land use planning (TEK17, 2017).

For the assessment of the quantitative risk of avalanches reaching existing settlements only limited methods are available. Thus, historical observations can be of special importance, as they may be direct indicators for the real hazard in the area of interest. To a certain degree, they can also provide an indication of a possible change of hazard over time due to environmental changes. However, historical observations are affected by inherent uncertainties and many questions remain open.

Here, we aim to combine results from several work packages to develop a more consistent method of using historical observations that may help improve quantitative hazard assessments and evaluation of the uncertainties involved.

2 Research goals

The avalanche hazard is affected by several factors, for example:

- terrain (slope, shape, exposure, ...)
- ground conditions
- vegetation (ground cover, density of forest, ...)
- precipitation (frequency, intensity, snow or rain, ...)
- the influence of the wind (drift snow deposition, intensity of loading, or cornices)
- snow cover properties (maritime versus continental climate, ...)
- runout length for avalanches

All these parameters have variations that can be described by probability distributions. In hazard assessments, the task is to determine the location of a boundary that delineates a zone with a given nominal annual exceedance probability. To this end, a common simplification is often used to quantify the annual avalanche hazard / avalanche probability Haz(s) for an area at the location s that is to be assessed (e.g. McClung, 2000; Schläppy et al., 2014):

$$Haz(s) = P_R \cdot P_s \,. \tag{1}$$

Here, P_R denotes the avalanche probability (or frequency, $P_R \approx \lambda$) for avalanches with a runout length longer than a threshold s_0 and P_s denotes the probability that the avalanche

also reaches or passes the area of interest at the location s (the probability of exceeding s). The runout length, s, is measured along the terrain profile of the avalanche path.

The research goal is to quantify the uncertainty involved in the delimitation of hazard zones in the light of historical events using Eq (1). Eq (1) combines two probabilities, which both are fraught with uncertainties. The uncertainties in the delimitation of hazard zones can be temporal as well as spatial.

3 Methods

To demonstrate the uncertainties involved in the hazard assessment, we deploy a fictitious example (but with a realistic background). For simplicity, let us assume a parabolic track. Furthermore, without loss of generality, let us assume that the mean of the observed runout distances corresponds to the α-point (Lied & Bakkehøi, 1980) at the location s_α along the track and that average return period (i.e. the reciprocal of the probability) corresponding to this mean is about 100 years, (i.e. $Haz(s_\alpha) = 0.01$). We also assume an observed avalanche history for the track reaching back to the year 1650.

Table 1 Fictitious avalanche history (HSC is the total potential drop height of the track).

date	observed runout length s scaled by H_{SC}	observed drop height ΔH scaled by H_{SC}	retarding acceleration a_{ret} scaled by g
1665-12-28	2.391	1	-0.418
1741-12-10	2.427	1	-0.412
1795-01-27	2.017	0.99	-0.486
1818-02-22	2.576	1	-0.388
1858-01-12	2.006	0.98	-0.488
1952-03-21	2.010	0.98	-0.488
1958-12-19	2.038	0.98	-0.483
1990-02-11	2.257	1	-0.443

In our example, the runout distribution of the mean retarding acceleration:

$$a_{ret} = -g\frac{\Delta H}{s}, \tag{2}$$

follows a Gumbel-type extreme value distribution, which is often a reasonable approximation in the runout area of major avalanches (c.f. NGI 20170131-17-R, chapter 3.2). ΔH is the drop height, g the gravitational acceleration, and s is a given location along the track. However, the principal approach is not limited to a special distribution.

We also assume that the record is complete for all avalanches that surpassed a line at s_0 (in our example $s_0 \approx 1.57H_{SC}$).

According to Eq. (1) the determination of the avalanche hazard/probability Haz(s) at a location s is depending on two probabilities, the avalanche frequency and the runout probability distribution.

Based on our data, we derive an estimate on the avalanche frequency and the runout probability distribution and corresponding confidence intervals. Using these estimates, we present different approaches to estimate the associated uncertainties for the avalanche hazard at a location s, which can be interpreted as either spatial or temporal fuzziness.

4 Results

4.1 Avalanche frequency, λ

In our example, we consider eight major avalanches observed in the period between 1650 and 2021. This corresponds to a mean return period for avalanches surpassing the reference level s_0 of about 45 years. Figure 1 shows the calculated annual avalanche frequency λ based on those avalanche events and the corresponding 90%-confidence interval. The calculation follows the method suggested by Mudelsee (2020, Chapter 3), which also involves data sampling/bootstrapping to calculate the confidence interval. The occurrence rate/ avalanche frequency is calculated as:

$$\lambda(T) = h^{-1}\sum_{j=1}^{m} K\left(\left[T - T_{event}(j)\right]/h\right), \tag{3}$$

where h is the bandwidth, K is a suitable kernel function (e.g. a Gaussian kernel), m is the number of observed events and T are the dates of occurrence.

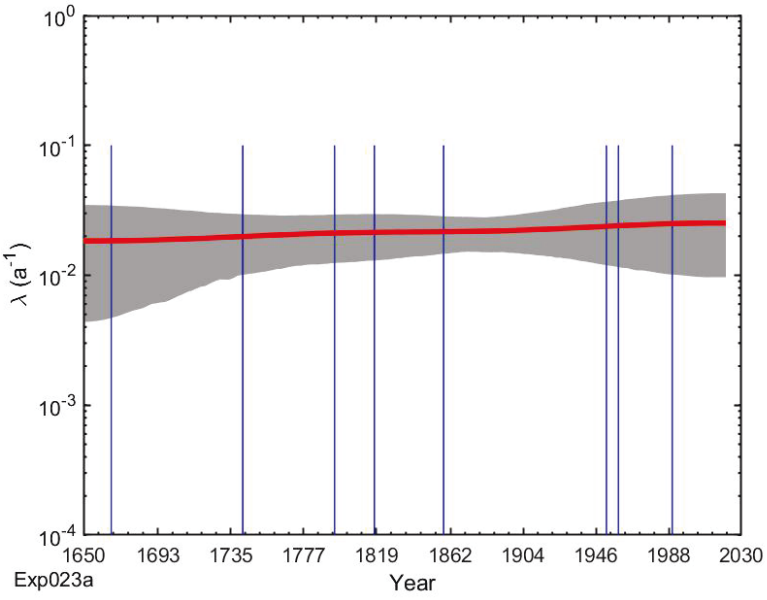

Figure 1 Estimated avalanche frequency λ over time. The gray area indicates the 90%-confidence interval.

The calculations suggest that with 90% confidence the avalanche frequency in 2021 is between 0.0115 and 0.0391 per year, with an expected value E(λ) = 0.0251 a^{-1}. This corresponds to a return period between around 26 and 87 years with an expected return period of about 40 years. In this example, the overall expected return period has been increasing slightly over time, with a return period of about 43 years ($\lambda \approx 0.0233 a^{-1}$) at the present time.

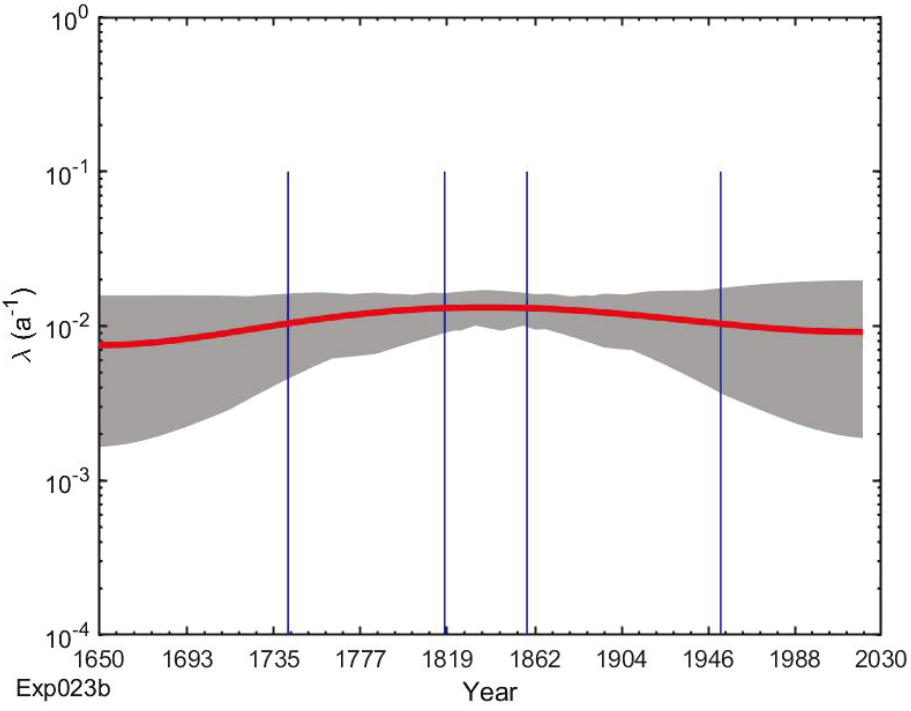

Figure 2 Estimated avalanche frequency λ over time for all avalanches surpassing s = s_α. The gray area indicates the 90%-confidence interval.

Approach T0: Figure 2 shows the calculated annual avalanche frequency λ based on those avalanche that surpassed a reference level s=s_α. In this case the expected frequency λ in 2021 is 0.0091 per year ($R_T \approx 109$ years) and the corresponding 90% -confidence interval is CI ≈ [0.0026, 0.01569] per year ($CI_{RT} \approx [64, 389]$ years).

These examples show that, although relatively many observations are available, the uncertainty defining the actual avalanche return period can be considerable due to the randomness in the occurrences.

4.2 Avalanche runout probability of exceedance, P_s

P_s denotes the probability that the avalanche also reaches or passes the area of interest at a location s (i.e. the probability of exceeding s) and is given by:

$$P_s = (1 - F(s \mid s \geq s_0)) = 1 - P_{ro}, \quad (4)$$

where, $F(s|s \geq s0)$ is the cumulative distribution function (CDF). Figure 3 shows the probability plot of a_{ret} in our example derived from the observations. a_{ret} is related to s.

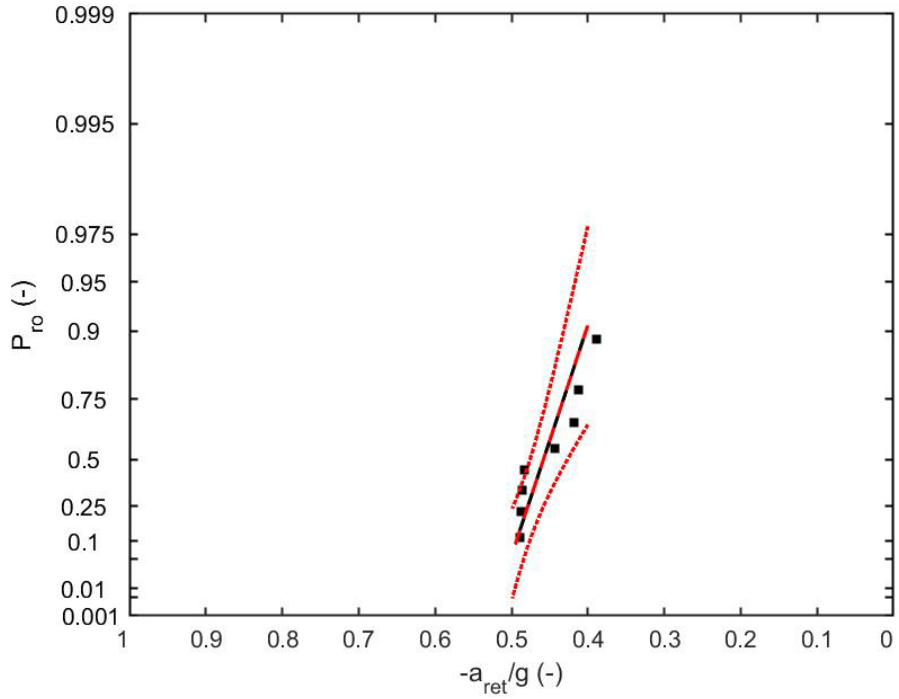

Figure 3 Probability plot of a_{ret}. The solid line shows the best fit and the dashed lines the 90%-confidence interval.

As stated above, in this example, we assume a Gumbel extreme value distribution in which case the quantile function is given by:

$$Q(P_{ro}) = \mu_e - \beta_e \ln\left(\ln\left(P_{ro}\right)\right), \tag{5}$$

where μ_e is the location parameter and β_e (> 0) is the scale parameter. The determination of both is also fraught with uncertainties. For the Gumbel distribution the following relations hold true:

$$\text{median} = \mu_e - \beta_e \ln(\ln(2)) \tag{6}$$

and

$$\text{mean} = \mu_e + \beta_e \gamma, \tag{7}$$

where the Euler–Mascheroni constant $\gamma = 0.5572$. Per definition, the probability P_{ro} corresponding to the median is 0.5 and Eq. (7) implies the probability P_{ro} corresponding to the mean is 0.5704. Using Eq. (6), the retarding acceleration corresponding to P_{ro} can be written as

$$a_{ret}(P_{ro}) = M(a_{ret}) - \beta_e \left(\ln(-\ln(P_{ro})) - \ln(-\ln(0.5))\right), \tag{8}$$

where $M(a_{ret})$ is the median of the observed a_{ret}.

4.3 Uncertainty

Based on our initial assumptions $P_{ro} = 0.5704$ and $\bar{\lambda} = 0.233$, in which case the mean avalanche hazard/probability at the location s_α is

$$Haz(s_\alpha) = \lambda \cdot P_s = \lambda \cdot (1 - P_{ro}) = 0.01,$$

as assumed. Eq (1) allows a closer look at the influence of the individual uncertainties. To this end, we also consider the variations

$$\lambda = \frac{Haz(s)}{1 - P_{ro}} \tag{9}$$

and

$$P_{ro} = 1 - \frac{Haz(s)}{\lambda} \tag{10}$$

All cases presuppose that $Haz(s) \le \lambda$. To compare the uncertainty regarding the return period, we consider the reference location $s = s_B$ of the expected position of boundary that delineates the zone with a given annual exceedance probability.

4.4 Spatial uncertainty due to uncertainty of the avalanche frequency

Approach S1: In a first step, we look at the spatial uncertainty in determining the position $s_{B1/100}$ corresponding to the boundary that delineates the zone with probability $Haz(s_{B1/100}) = 1/100$. We assume that in addition to the mean retarding acceleration $(\bar{a}_{ret}/g = -0.456)$, also know the scale parameter β_e is known (β_e.= 0.0242). As described above in our example, the calculated 90% confidence interval of the return period in the year 2021 ranges between 0.0115 and 0.0391 per year. Now using Eq. (10), we obtain $P_{ro} = [0.128, 0.7442]$ and further by using Eq. (8), $a_{ret}/g = [-0.4874, -04404]$, which can be related to a upper limit $s_{u1/100}$ and a lower limit $s_{l1/100}$ for position the boundary. In our example, the difference in the runout length is then $(s_{l1/100} - s_{u1/100})/H_{SC} = \Delta s_{B1/100}/H_{SC} \approx 0.26$, which is the width of the uncertainty range. Similarly, we can consider the upper limit $s_{u1/1000}$ and lower limit $s_{l1/1000}$ of the boundary position belonging to $Haz(s_{B1/1000}) = 1/1000$, in which case we obtain a difference of $\Delta s_{B1/1000}/H_{SC} = 0.19$.

Figure 4 depicts the example, where the black squares mark our fictious observations and the dots the so-called β- and α-point corresponding to the α-β model (Lied & Bakkehøi 1981).

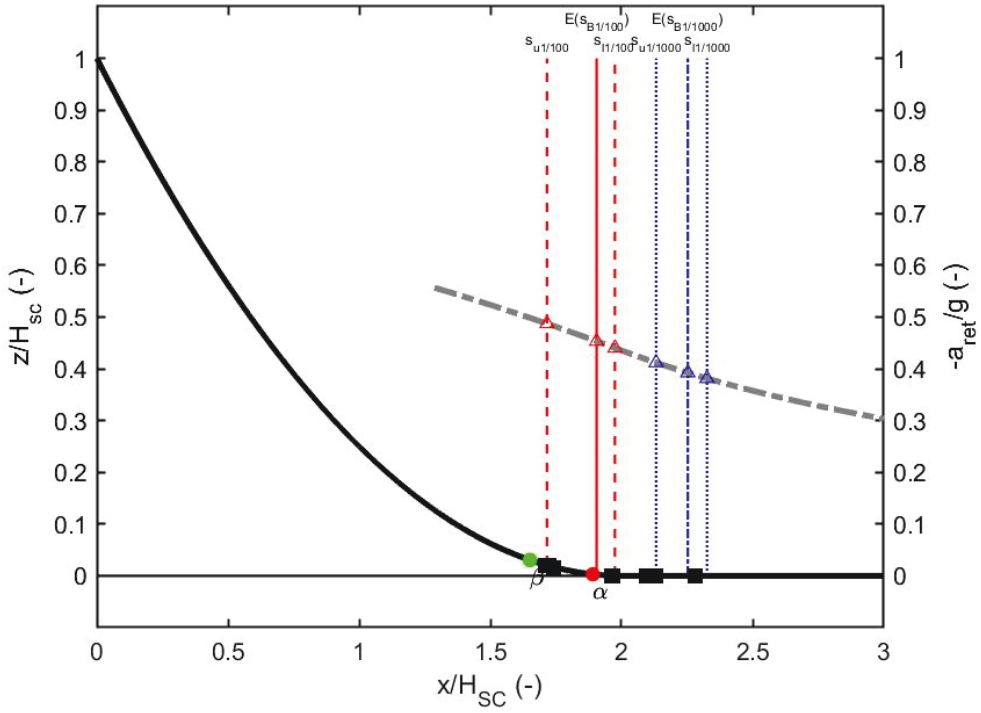

Figure 4 Idealized terrain profile along the avalanche path. For reference, the β- and α-point of the α-β model (Lied & Bakkehøi 1981) are given. Black squares mark the fictious estimates for observed runout lengths. The profile is scaled with total drop height H_{SC}. The gray dash-dotted line shows the retarding acceleration corresponding to the assumed profile. The solid red vertical line marks the expected boundary position $E(s_{B1/100})$ which delineates the zone with a probability $Haz(s_{B1/100}) = 1/100$ and the vertical blue dash-dotted line the position $E(s_{B1/1000})$ for $Haz(s_{B1/100}) = 1/1000$. The vertical red dashed lines and the vertical blue dotted depict the positions s_u and s_l of the 90% confidence interval of the respective zone boundaries. The triangles depict the respective retarding accelerations.

4.5 Uncertainty due to uncertainty in the runout distribution

Like the estimation of the avalanche frequency of a given set of observation is fraught with uncertainty, so is the determination of the runout distribution. Therefore, in the next step, we relax our assumption about the exact knowledge of the parameters of our Gumbel distribution and assume that only a normal distribution of the respective parameter is known. In our case, $\mu_e \approx N(-0.447, 0.0121)$ and $\beta_e \approx N(0.024, 0.006)$.

We now can use this knowledge in a Monte Carlo simulation to estimate the runout. Figure 5 shows the obtained distribution of the retarding acceleration (Eq (8)) versus P_{ro} for randomly chosen for μ_e. and β_e.

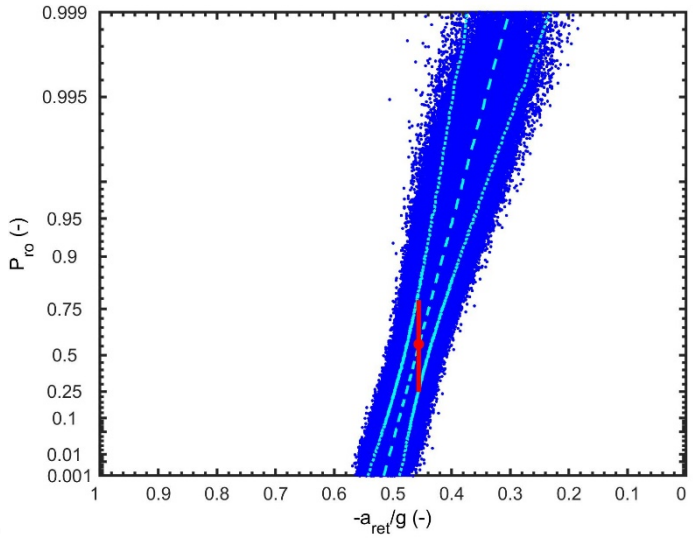

a)

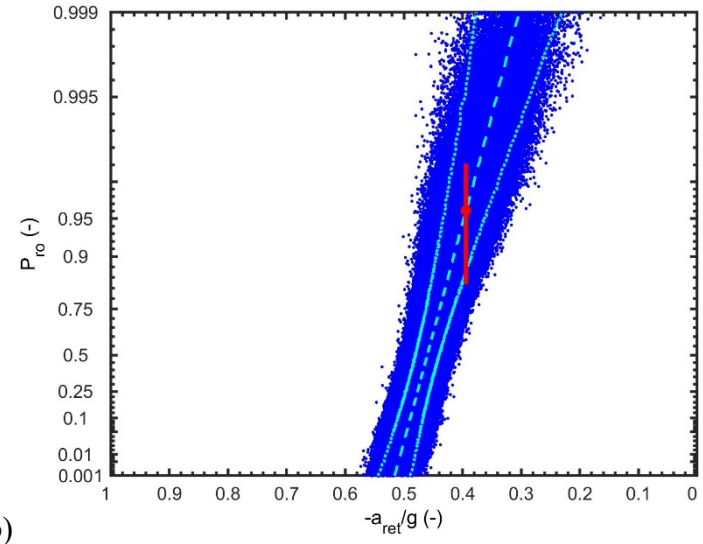

b)

Figure 5 Calculated a_{ret} /g depending on P_{ro} for given normal distributions for μ_e. and βe of a Gumbel distribution (blue dots). The dash cyan line depicts the approximated cumulative distribution function, and the dotted cyan lines represent the 90% confidence interval. a) The red dot marks the expected mean value of the retarding acceleration, that corresponds to the expected boundary position E(sB1/100) delimiting the zone with a probability Haz(sB1/100) = 1/100. The vertical solid red line marks the 90%-confidence interval of all Pro with $a_{ret}(P_{ro}) \approx \bar{a}_{ret}$. b) The same as a) expect considering the expected position E(sB1/1000) delimiting the zone with Haz(sB1/1000) = 1/1000.

The results of the Monte Carlo simulation can be interpreted in slightly different ways in respect to the assessment of hazard zones.

4.5.1 Temporal fuzziness

Approach T1: First, we consider the probability given as ratio of the number of all realizations N_B with $a_{ret} > a_{ret}(s_{B1/100})$ to the total number of simulations N_{tot}. This corresponds to the probability of exceeding the given location $s_{B1/100}$. In our example, $N_{B1/100}/N_{tot} \approx 0.449$. Combining this with the calculated confidence interval of the avalanche frequency λ suggests that the annual avalanche probability is in the range $Haz(s_{B1/100}) \approx [0.0051, 0.0176]$, which corresponds to a 90%-confidence interval for the return period $R_T(s_{B1/100}) \approx [57, 195]$ years.

Approach T2: Another way to look at the uncertainty involved is to consider the 90%-confidence interval of the realization $a_{ret}(P_{ro}) \approx a_{ret}(s_{B1/100})$, which in our example is $P_{ro} \approx [0.2536, 0.7806]$. By combing this with the expected avalanche frequency in 2021 one obtains a second proxy for the uncertainty of the annual avalanche probability $Haz(s_{B1/100}) \approx [0.0051, 0.0174]$ or $R_T(s_{B1/100}) \approx [57, 196]$ years.

Similarly, we can evaluate the uncertainties related to the delimitation of the boundary position $s_{B1/1000}$ of the zone with $Haz(s_{B1/1000}) = 1/1000$. For our example, the ratio of number of all realizations N_B with $a_{ret} > a_{ret}(s_{B1/1000})$ to the total number of simulations is $N_{B1/1000}/N_{tot} \approx 0.052$. This combined with the calculated confidence interval of the annual avalanche frequency λ suggests $Haz(s_{B1/1000}) \approx [6 \cdot 10^{-4}, 0.0021]$ or $R_T(s_{B1/1000}) \approx [488, 1663]$ years.

Or on the other hand using the 90%-confidence interval of the realization $a_{ret}(P_{ro}) \approx a_{ret}(s_B)$ $P_{ro} \approx [0.838, 0.983]$. Again, combining this with the expected avalanche frequency λ, in 2021, suggests the that range for the annual avalanche probability $Haz(s_{B1/1000}) \approx [4 \cdot 10^{-4}, 0.0038]$ corresponding to a range of return period $R_T(s_{B1/1000}) \approx [265, 2500]$ years.

4.5.2 Spatial fuzziness

Approach S2: Now, let us consider the uncertainty in the determination the expected boundary position $E(s_B)$ delimiting the zone with a probability $Haz(s_B)$ is only related to the uncertainty in the runout distribution. Figure 6 shows the calculated values of a_{ret}/g, where the red lines show the 90%-confidence interval for a_{ret} of realization for $P_{ro} = 0.5708$ and $P_{ro} = 0.9571$, which would correspond to the expected annual avalanche probabilities $Haz(s_B)$ of 1/100 and 1/1000 respectively.

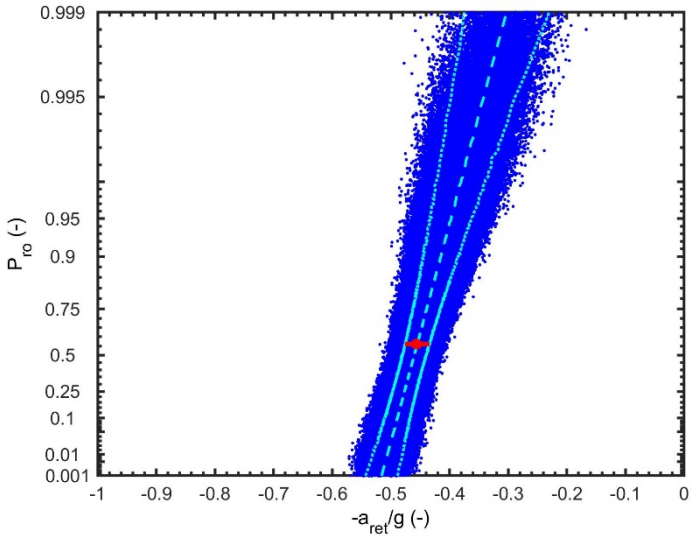

a)

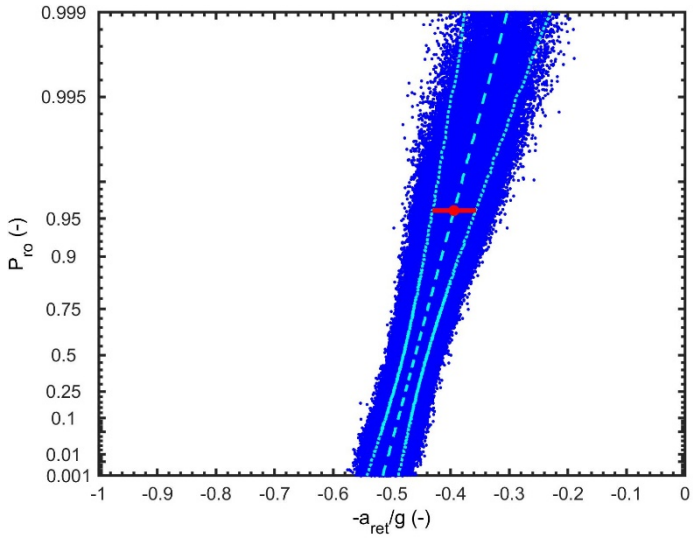

b)

Figure 6 Calculated a_{ret}/g depending on P_{ro} for given normal distributions for μ_e. and β_e of a Gumbel distribution (blue dots). The dash cyan line depicts the approximated cumulative distribution function, and the dotted cyan lines represent the 90% confidence interval. a) The red dot marks the expected mean value of the retarding acceleration that corresponds to the expected boundary position $E(s_{B1/100})$ delimiting the zone with an annual probability $Haz(s_{B1/100}) = 1/100$. The horizontal red line marks the 90%-confidence interval of all $a_{ret}(P_{ro})$ for given $P_{ro} = 0.5708$ b) The same as a) except considering $Haz(s_{B1/1000}) = 1/1000$ that is $P_{ro} = 0.9571$.

Figure 6 illustrates the variations of the retarding acceleration a_{ret} for a given runout probability P_{ro} and therefore the variation of boundary position s_B delimiting the zone with a given avalanche probability $Haz(s_B)$. In this example, the 90%-confidence interval for the boundary position $s_{B1/100}$ delimiting the zone with an annual probability

Haz($s_{B1/100}$) = 1/100 spans a range of $\Delta s_{B1/100} \approx 0.23 H_{SC}$ and the boundary position for the zone Haz($s_{B1/1000}$) = 1/1000 a range of $\Delta s_{B1/1000} \approx 0.48 H_{SC}$.

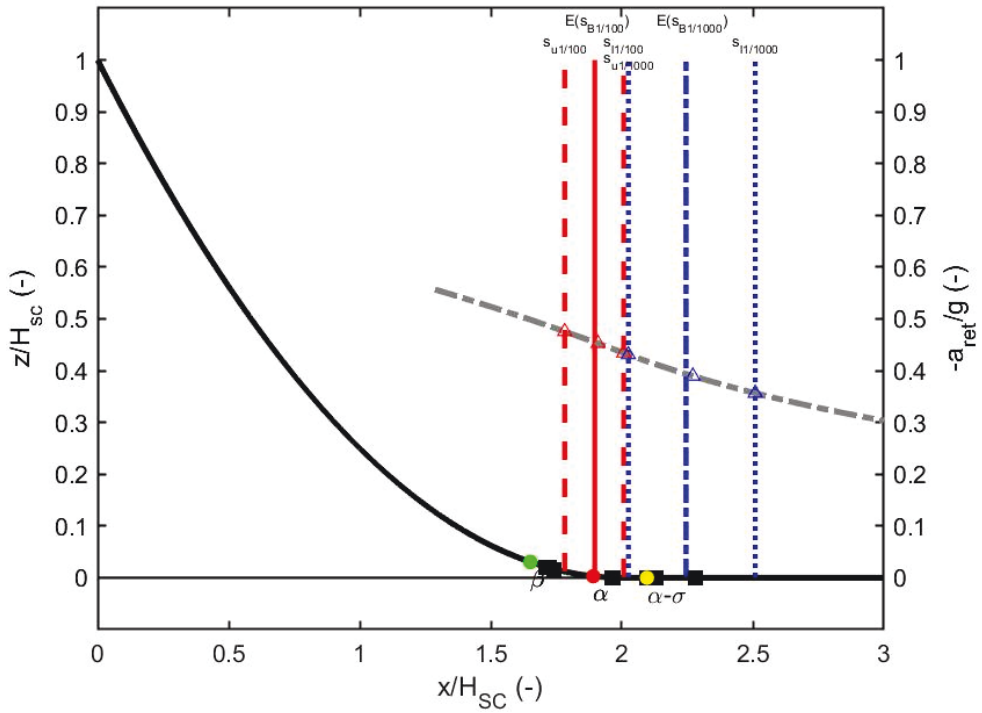

Figure 7 Idealized terrain profile along the avalanche path. For reference, the β-, α- and (α-σ) -point of the α-β model (Lied & Bakkehøi 1981) are given. Black squares mark the fictious estimates for observed runout lengths. The profile is scaled with total drop height H_{SC}. The gray dash-dotted line shows the retarding acceleration corresponding to the assumed profile. The solid red vertical line marks the expected boundary position $E(s_{B1/100})$ of the zone with an annual avalanche probability $HAZ(s_{B1/100}) = 1/100$ and the vertical blue dash-dotted line the position $E(s_{B1/1000})$ of that with $HAZ(s_{B1/1000}) = 1/1000$ based on a Monte-Carlo simulation. The vertical red dashed lines and the vertical blue dotted depict the positions s_u and s_l of the 90% confidence interval of the respective zone boundaries. The triangles depict the respective retarding accelerations.

4.6 Full Monte-Carlo approach for delimiting the hazard zone boundary

In a last trial we relax our previous assumption once more and assume that the estimate for the avalanche frequency in 2021 also follows a normal distribution $\lambda(2021) \approx N(0.0252, 0.0103)$. Now we also include this information in our Monte-Carlo approach. Again, we can relate the uncertainty involved in the delimitation of boundary position s_B that delineates the zone with a given probability Haz(s_B) either to a "temporal" or to a "spatial" one.

Approach T3: In the first case, the calculated range for the annual avalanche probability at a given position $s_{B1/100}$ becomes $Haz(s_{B1/100}) \approx [0.0022, 0.023]$ or $R_T(s_{B1/100}) \approx [44, 452]$ years.

The calculated range for the annual avalanche probability at a given position $s_{B1/1000}$ becomes $Haz(s_{B1/1000}) \approx [1.9 \cdot 10^{-4}, 0.0045]$ or $R_T(s_{B1/1000}) \approx [222, 5720]$ years.

Approach S3: In the second case, the 90%-confidential interval for the delimitation of the $s_{B1/100}$ spans a range of $\Delta s_{B1/100} \approx 0.35 H_{SC}$ and for $s_{B1/1000}$ spans a range of $\Delta s_{B1/1000} \approx 0.62 H_{SC}$. Figure 8 depicts our example applying a full Monte-Carlo approach.

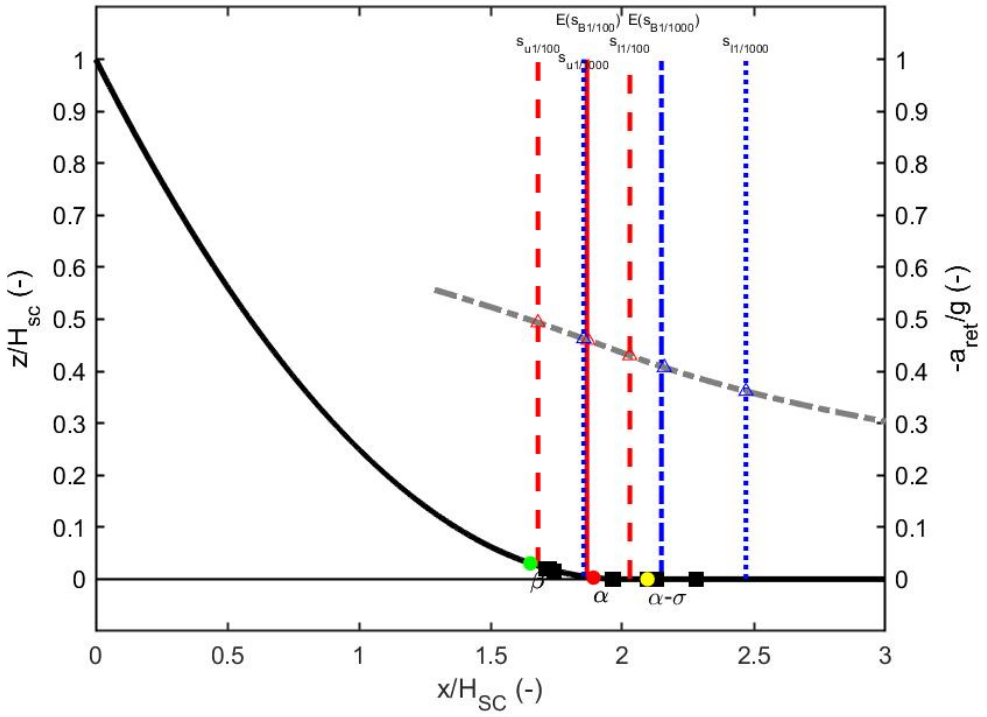

Figure 8 Idealized terrain profile along the avalanche path. For reference, the β-, α- and (α -σ) -point of the α-β model (Lied & Bakkehøi 1981) are given. Black squares mark the fictious estimates for observed runout lengths. The profile is scaled with total drop height H_{SC}. The gray dash-dotted line shows the retarding acceleration corresponding to the assumed profile. The solid red vertical line marks the expected boundary position $E(s_{B1/100})$ of the zone with an annual avalanche probability $HAZ(s_{B1/100})$ = 1/100 and the vertical blue dash-dotted line the position $E(s_{B1/1000})$ of that with $HAZ(s_{B1/1000})$ = 1/1000 based on a full Monte-Carlo simulation. The vertical red dashed lines and the vertical blue dotted depict the positions s_u and s_l of the 90% confidence interval of the respective zone boundaries. The triangles depict the respective retarding accelerations.

5 Concluding remarks

The example shows that even with a series of observations over a long time, the uncertainty in drawing a boundary line for a hazard zone with a given annual probability can still be considerable. The uncertainties can either be interpreted as related to the expected return periods or as spatial fuzziness.

Table 2 and Table 3 give a summary of the spatial and temporal fuzziness, respectively, as illustrated by the various approaches described in our example.

Table 2 Summary spatial fuzziness

Approach	$\Delta s_{B1/100}/H_{SC}$	$\Delta s_{B1/1000}/H_{SC}$
S1	0.26	0.19
S2	0.23	0.48
S3	0.35	0.62

Table 3 Summary temporal fuzziness (return period R_T in years).

Approach	$R_T(s_{B1/100})$	$R_T(s_{B1/1000})$
T0	[64, 389]	
T1	[57, 195]	[488, 1663]
T2	[57, 196]	[265, 2500]
T3	[44, 452]	[222, 5720]

The calculations above suggest that the estimates of expected return periods solely based on historical observations as input for the hazard zoning, even when based on well documented events, should be regarded as being within an order of magnitude. This interpretation was already made by Mears in 1992. An overly detailed delimitation of avalanche hazard zones boundaries based on these estimates can be counterproductive because it can give a false impression of accuracy.

The above remark is in many aspects also valid for modelling approaches. This in turn suggests that derived nominal probabilities should also regard as being within an order of magnitude rather than an exact value.

6 References

Mudelsee, M. (2020) Statistical Analysis of Climate Extremes Cambridge University Press, 2020

Lied, K. & Bakkehøi, S. (1980) Empirical calculations of snow-avalanche run-out distance based on topographic parameters Journal of Glaciology, 1980, 26, 165-177

McClung, D. M. (2000). Extreme avalanche runout in space and time. Canadian Geotechnical Journal 37, 161–170.

Mears, A.:(1982) Snow-Avalanche Hazard Analysis for Land-use Planning and Engineering, Colorado Geological Survey, Dept. of Natural Resources, State of Colorado, Surv. Bulletin 49

NGI 20170131-17-R Issler, D.; Gauer, P.; Glimsdal, S.; Jaedicke, C.; Sandersen, F. & Gisnås, K. G. (2020) SP4 FoU Snøskred-ANNUAL REPORT 2019 Norwegian Geotechnical Institute, Norwegian Geotechnical Institute, 2020

Schläppy, R., Eckert, N., Jomelli, V., Stoffel, M., Grancher, D., Brunstein, D., Naaim, M. and Deschatres, M. (2014). Validation of extreme snow avalanches and related return periods derived from a statistical-dynamical model using tree-ring techniques. Cold Regions Science and Technology 99, 12–26.

TEK17, Byggteknisk forskrift (2017) Veiledning Direktoratet for byggkvalitet, Direktoratet for byggkvalitet, 2017

Kontroll- og referanseside/ Review and reference page

Dokumentinformasjon/*Document information*		
Dokumenttittel/*Document title* CPT 3 – Quantitative risk assessment: Remarks on the uncertainty in the delimitation of hazard zones based on historical observations		**Dokumentnr./*Document no.*** 20200017-09-TN
Dokumenttype/*Type of document* Teknisk notat / Technical note	**Oppdragsgiver/*Client*** NVE	**Dato/*Date*** 2022-03-22
Rettigheter til dokumentet iht kontrakt/ *Proprietary rights to the document according to contract* Oppdragsgiver / Client		**Rev.nr.&dato/*Rev.no.&date*** 0 /
Distribusjon/*Distribution* ÅPEN: Skal tilgjengeliggjøres i åpent arkiv (BRAGE) / OPEN: To be published in open archives (BRAGE)		
Emneord/*Keywords* Norwegian avalanche_grant, uncertainty, hazard maps, snow avalanches, runout distances, return period, frequency		

Stedfesting/*Geographical information*	
Land, fylke/*Country* Norway	**Havområde/*Offshore area***
Kommune/*Municipality*	**Feltnavn/*Field name***
Sted/*Location*	**Sted/*Location***
Kartblad/*Map*	**Felt, blokknr./*Field, Block No.***
UTM-koordinater/*UTM-coordinates* **Zone: East: North:**	**Koordinater/*Coordinates*** **Projection, datum: East: North:**

Dokumentkontroll/*Document control*
Kvalitetssikring i henhold til/*Quality assurance according to NS-EN ISO9001*

Rev/ *Rev.*	**Revisjonsgrunnlag/*Reason for revision***	**Egenkontroll av/ *Self review by:***	**Sidemanns-kontroll av/ *Colleague review by:***	**Uavhengig kontroll av/ *Independent review by*:**	**Tverrfaglig kontroll av/ *Inter-disciplinary review by:***
0	Original document	2022-03-22 Peter Gauer	2022-02-28 Krister Kristensen	2022-03-22 Christian Jaedicke	

Dokument godkjent for utsendelse/ *Document approved for release*	**Dato/*Date***	**Prosjektleder/*Project Manager***
	22 March 2022	Christian Jaedicke

NGI (Norwegian Geotechnical Institute) is a leading international centre for research and consulting within the geosciences. NGI develops optimum solutions for society and offers expertise on the behaviour of soil, rock and snow and their interaction with the natural and built environment.

NGI works within the following sectors: Offshore energy – Building, Construction and Transportation – Natural Hazards – Environmental Engineering.

NGI is a private foundation with office and laboratories in Oslo, a branch office in Trondheim and daughter companies in Houston, Texas, USA and in Perth, Western Australia

www.ngi.no

NGI (Norges Geotekniske Institutt) er et internasjonalt ledende senter for forskning og rådgivning innen ingeniørrelaterte geofag. Vi tilbyr ekspertise om jord, berg og snø og deres påvirkning på miljøet, konstruksjoner og anlegg, og hvordan jord og berg kan benyttes som byggegrunn og byggemateriale.

Vi arbeider i følgende markeder: Offshore energi – Bygg, anlegg og samferdsel – Naturfare – Miljøteknologi.

NGI er en privat næringsdrivende stiftelse med kontor og laboratorier i Oslo, avdelingskontor i Trondheim og datterselskaper i Houston, Texas, USA og i Perth, Western Australia.

www.ngi.no

OSLO
TRONDHEIM
HOUSTON
PERTH

NORWEGIAN GEOTECHNICAL INSTITUTE
NGI.NO

Main office
PO Box 3930 Ullevaal St.
NO-0806 Oslo
Norway

Trondheim office
PO Box 5687 Torgarden
NO-7485 Trondheim
Norway

T (+47)22 02 30 00
F (+47)22 23 04 48
NGI@ngi.no

BIC NO. DNBANOKK
IBAN NO26 5096 0501 281
ORGANISATION NO.
958 254 318MVA